Environmental Science & Technology

Article

pubs.acs.org/est

Hydrodynamic Forcing Mobilizes Cu in Low-Permeability Estuarine Sediments

Minwei Xie,[†,‡] Ning Wang,[†,‡] Jean-François Gaillard,[*,†] and Aaron I. Packman[*,†]

[†]Department of Civil and Environmental Engineering, Northwestern University, 2145 Sheridan Road, Evanston, Illinois 60208-3109, United States

[‡]Faculty of Geosciences and Environmental Engineering, Southwest Jiaotong University, Chengdu, Sichuan 610031, China

Supporting Information

ABSTRACT: Overlying hydrodynamics play critical roles in controlling surface-porewater exchanges in permeable sediments, but these effects have rarely been characterized in low-permeability sediments. We conducted a series of laboratory experiments to evaluate the effects of varied hydrodynamic conditions on the efflux of metals from low-permeability estuarine sediments. Two Cu-contaminated sediments obtained from the Piscataqua River were subject to controlled levels of hydrodynamic shear in Gust mesocosms, including episodic sediment resuspension. Overlying water and porewater samples were collected over the course of experiments and analyzed for metal concentrations. The two sediments had similar permeability ($\sim 10^{-15}$ m^2), but different particle size distributions. Hydrodynamic forcing enhanced the mobilization and efflux of Cu from the coarser-grained sediments, but not the finer-grained sediments. Sediment resuspension caused additional transitory perturbations in Cu concentrations in the water column. Particulate metal concentrations increased significantly during resuspension, but then rapidly decreased to preresuspension levels following cessation of sediment transport. Overall, these results show that the mobility and efflux of metals are likely to be influenced by overlying hydrodynamics even in low-permeability sediments, and these effects are mediated by sediment heterogeneity and resuspension.

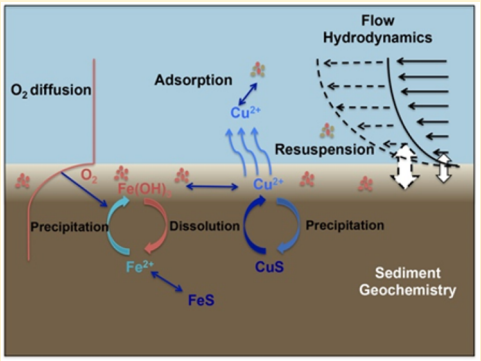

INTRODUCTION

Estuaries represent transitions between riverine and marine environments.[1] Estuaries receive inputs of fresh water, weathered materials, nutrients and contaminants from terrestrial environments. Estuaries are also strongly influenced by tidal currents from the ocean. At flood tide, saline water is forced into many estuaries, while outflows to the ocean increase at ebb tide.[2] Mixing of fresh and marine water retains and recycles particulate matter and nutrients within estuarine environments. Because of their dynamic and retentive characteristics, estuaries rank among the most productive ecosystems on earth and provide habitats for a variety of aquatic life.[3,4]

Metal contaminants entering into estuaries are transferred from water into sediments by many processes, most notably precipitation, adsorption, and sedimentation. The resulting metal-contaminated sediments then act as potential sources to the water column, posing ongoing threats to the aquatic environment. Some metals such as Cu are essential elements for a variety of metabolic processes, but also show toxicity when overabundant.[5,6] Sublethal effects for bacterial cells, algae, aquatic invertebrates, and fishes begin to appear when the Cu concentration exceeds 5 μg/L.[5]

The mobility of metals in sediments is controlled by a wide range of factors, including redox distribution, pH, and salinity.[7,8] These factors are known to vary with transport and mixing processes such as hyporheic exchange, bioturbation, and bioirrigation.[9−14] Hyporheic exchange—exchange of porewater with the overlying water column—directly influences mass transfer of both solutes and particulate matter across the sediment-water interface (SWI).[15] Advective porewater flows influence a wide range of sedimentary biogeochemical processes, including metals speciation and contaminant biodegradation.[16−22] However, the effects of hyporheic exchange and porewater flow on contaminant dynamics are frequently neglected in low-permeability sediments, as molecular diffusion is generally considered to be the dominant porewater transport process in these sediments.[19,22−26] Field investigations have shown that both waves and currents enhance transport of solutes such as nutrients, silica, and oxygen across the SWI in estuaries and coastal oceans.[27−29] Tidal cycles also alter redox conditions and affect the mobility of metals in sediments.[29,30] Metals are enriched in fine sediment particles and total metal concentrations in sediments are normally orders of magnitude higher than those in

Received: September 18, 2015
Revised: April 5, 2016
Accepted: April 7, 2016

DOI: 10.1021/acs.est.5b04576
Environ. Sci. Technol. XXXX, XXX, XXX−XXX

porewater and overlying water.[31] Small changes in sediment geochemical conditions may thus exert significant effects on exchange of metals between sediments and waters. In a previous study, we found that sediment resuspension transiently changed the speciation of Zn in surficial sediments and significantly promoted the liberation of Zn to the porewater and overlying water column.[32]

Accordingly, we hypothesize that hydrodynamic forcing enhances the mobility of metals even in low-permeability sediments and the overall liberation of metals to the water column. To test this hypothesis and improve understanding of hydrodynamic controls on metals efflux from low-permeability contaminated sediments, we conducted Gust chamber experiments with Cu-contaminated estuarine sediments. We evaluated Cu releases to porewater and overlying water under a range of hydrodynamic conditions, including steady flows without sediment resuspension and time-varying flows with episodic sediment resuspension. We then evaluated the mechanisms by which overlying and porewater flows mobilized metals.

MATERIAL AND METHODS

Sample Collection. Metals-contaminated sediments were obtained from Portsmouth Naval Shipyard (PNS), a U.S. Navy shipyard located at the mouth of Portsmouth Harbor (Figure S1, Supporting Information). Portsmouth harbor is predominantly saline and exhibits current velocities from 1.5 to 2 m/s. Sediments used in the laboratory experiments presented here were collected from PNS monitoring stations MS3 and MS4 in September of 2012. ∼ 15 cm of surficial sediments were collected manually by divers and then shipped overnight in coolers to the laboratory, and refrigerated at 4 °C until used in the experiments.

Sediment Characterization. Bulk sediment properties, including porosity, porewater conductivity and salinity, particle size distribution, permeability, total organic carbon, acid volatile sulfide (AVS), simultaneously extracted metals (SEM), and total metal concentrations were measured on homogenized sediment samples. Bulk porosity was measured by drying 10 cm^3 of sediments at 70 °C for 48 h, and then converting the weight loss of water to volume fraction. Porewater was extracted by centrifuging the sediments at 3414*g* for 20 min (Legend RT plus, Thermo Scientific). Conductivity of the filtered supernatant (0.2 μm nylon filter, VWR International) was measured with a conductivity probe (Oakton Con 11, Cole-Parmer). Ten mL of the supernatant was dried at 70 °C for 48 h and the salinity was determined by measuring the weight of the remaining solids. Sediment grain size distribution was measured by wet-sieving with 45, 106, 150, 250, and 1000 μm sieves and measuring the dry weight. Permeability was measured in a constant-head permeameter with a test section of 2.5 cm in diameter and 5 cm in length (column and fittings from Omnifit Ltd.) Bulk AVS and SEM were determined by the 1 M cold HCl extraction and 0.5 M NaOH trap technique (Supporting Information).[33] Total organic carbon was measured by acidifying 80 mg of dry sediments with 1.5 mL of 4 M HCl followed by analysis with an elemental analyzer (ECS 4010, Costech Analytical Technologies, Inc.) Total bulk metal concentrations were measured using ICP-AES (Vista-MPX, Varian) after microwave-assisted acid digestion following U.S. Environmental Protection Agency method 3051A.[34]

Experimental Setup. Gust-type mesocosms[35] were used to subject the PNS sediments to controlled overlying flow conditions. The Gust chamber (Green Eyes LLC) (Figure S2, Supporting Information) uses a combination of a spinning disk and a central suction port to generate uniform shear stresses over the SWI. A DC power supply and a linear motor controller (LSC 30/2, Maxon Motor) precisely control the rotation rate of the spinning disk, providing calibrated shear stresses between 0.01 and 0.90 Pa. All parts of the Gust chamber were made of polycarbonate to minimize metal contamination. A covered 5 L plastic beaker was used as a reservoir for recirculating water. The inlet and outlet ports of the Gust chamber were connected to the water reservoir by Tygon tubing (VWR International) and a peristaltic pump (Masterflex, Cole Parmer). Water in the reservoir was constantly mixed to ensure homogeneous distribution of dissolved and particulate material in recirculating water throughout the experiments. Rhizon *in situ* samplers[36−38] (RISS) with 0.15 μm pores (Sunvalley Solutions Inc.) were installed into the Gust chamber to enable time-series sampling of porewater over the course of the experiments. Experiments were performed with artificial seawater (ASW) made by dissolving 32 g sea salt (Tropic Marin) into 1 L Milli-Q water (Millipore).

Hydrodynamic Conditions. Six Gust chamber experiments were performed on PNS sediments. Hydrodynamic conditions for experiments (Table 1) were chosen relative to the critical shear (CS), which is the shear required to cause significant sediment resuspension. The critical shear of the sediments was first characterized by varying the shear stresses in a stepwise fashion until the turbidity of the overlying water significantly increased. The critical shear of both PNS sediments (MS3 and MS4) was 0.37 Pa (Figure S3, Supporting Information). Experiments were performed by imposing constant ("baseline") shears for 14 days. Separate experiments were run with baseline conditions at 3%, 50%, and 70% of the critical shear. Experiments run at 70% of the critical shear were also subject to two periods of episodic resuspension of 4 h duration each on days 1 and 8. Resuspension was achieved by subjecting the sediments to a constant shear of 0.90 Pa for 4 h.

Table 1. Conditions for Gust Chamber Experiments; All Experiments Had Durations of 14 Days

series	no.	sediment location	baseline shear (Pa)	% of critical shear	time of 4 h sediment resuspension	
F	F1	MS4	0.01	3		
	F2	MS4	0.19	50		
	F3	MS4	0.26	70	day 1	day 8
C	C1	MS3	0.01	3		
	C2	MS3	0.19	50		
	C3	MS3	0.26	70	day 1	day 8

Experimental Procedure. Before each experiment, all parts of the Gust chamber systems were cleaned by soaking in 10% HNO_3 (v/v) for 24 h and then rinsing with Milli-Q water. 800 mL of homogenized sediments were then carefully emplaced into the Gust chamber to form a 10 cm deep sediment bed with a flat surface. Three RISS were inserted into the sediment at depths of 1, 2, and 4 cm below the SWI while the sediment was introduced. The 10 cm of headspace was then slowly filled with ASW to avoid disturbance of the sediments. The erosion head was then placed onto the chamber. The system was allowed to stabilize overnight, and then 4.785 L

DOI: 10.1021/acs.est.5b04576
Environ. Sci. Technol. XXXX, XXX, XXX−XXX

ASW was continuously recirculated for 14 days under the hydrodynamic conditions listed in Table 1. The recirculating water was kept oxygenated during the experiments by continuously bubbling water-saturated air into the reservoir.

Sampling and Analysis. Dissolved oxygen (DO), pH, turbidity, and conductivity, dissolved and total metal concentrations in the recirculating water were measured daily. DO was measured directly in the water reservoir with a DO probe (HQ10, Hach). Twenty-four mL of overlying water was sampled from the recirculating flow daily and split into three aliquots. One aliquot of the overlying water was used to measure pH (420Aplus, Thermo Orion), conductivity, and turbidity (2100Q, Hach) and was returned to the water reservoir following analysis. The other two aliquots were analyzed for dissolved and total metal concentrations and an equal volume (16 mL) of clean ASW was added to the water reservoir to maintain a constant reservoir volume throughout the experiments. Samples analyzed for dissolved metals were filtered through a 0.2 μm filter (nylon, VWR International) and acidified with concentrated, trace-metal grade HNO_3 (Sigma-Aldrich) to pH < 2. Samples analyzed for total metals were acidified to pH < 2 without filtration. Samples were stored at 4 °C until analyzed. Samples for total metals were filtered just before analysis to remove any residual particulate matter.

Porewater samples were extracted via RISS on days 0, 1, 3, 5, 8, 10, 12, and 14. The first mL of porewater withdrawn from each RISS was discarded and then another 2 mL of porewater was collected, acidified to pH < 2, and stored for metal analysis.

Cu concentrations in overlying water and porewater samples were analyzed by Zeeman Graphite Furnace Atomic Absorption Spectrometry (Z-GFAAS, SpectrAA-800, Varian) (Supporting Information). Fe concentrations in overlying water samples were analyzed using the ferrozine colorimetric method.[39,40]

At the end of each experiment, the erosion head was removed and dissolved oxygen concentration profiles in porewater were measured with an oxygen microelectrode (OX-50, Unisense). In order to determine the variation of DO consumption rates with depth, we used the computer code PROFILE,[41] which fits the distribution of O_2 to a 1D steady-state transport-reaction equation. The overlying water was then drained, and a set of sediment subcores was obtained for AVS and SEM analysis using modified 60 mL syringes (Supporting Information).[42]

Dissolved Cu Efflux Model. The mass conservation equation that relates the release of $[Cu]_d$ from the porewater to the overlying water is

$$\frac{d[Cu]_{d,OW}(t)}{dt} = \alpha_{eff}\cdot[[Cu]_{d,SPW}(t) - [Cu]_{d,OW}(t)] \quad (1)$$

where the subscript OW indicates overlying water, SPW indicates surficial porewater, and t is the elapsed time. The effective mass transfer coefficient α_{eff} is defined by

$$\alpha_{eff} = D_{eff}\frac{A}{V}\frac{1}{\Delta z} \quad (2)$$

where D_{eff} is the effective diffusion coefficient, A the surface area of the SWI, Δz the depth of the source of $[Cu]_d$ in porewater, and V the volume of recirculating overlying water.

As a simplified case, assuming that the porewater $[Cu]_{d,SPW}(t)$ has a constant concentration S_0 throughout the experiment, and the analytical solution to eq 1 is

$$[Cu]_{d,OW}(t) = S_0 - B_0\cdot e^{-\alpha_{eff}\cdot t} \quad (3)$$

where $B_0 = S_0 - [Cu]_{d,OW}(t = 0)$.

For all experiments, nonlinear least-squares fitting was performed with eq 3 to obtain parameters S_0, B_0, and α_{eff}. For experiments F1–F3, and C1–C2, a single fitting was applied to the entire time-series of observed overlying water concentrations. For experiment C3, distinct trends in overlying concentrations were observed before and after the second resuspension (cf. Figure 2), so piecewise curve fitting was performed accordingly, as detailed in the SI.

RESULTS

Sediment Characteristics. Bulk sediment properties are shown in Table 2 and Figure 1. Both sediments had a significant fraction of very fine particles (<45 μm) (Figure 1). Sediments are identified by their relative size: C series sediments are coarser and more heterogeneous ($d_{50} \approx 150$ μm), while F series are finer and more homogeneous ($d_{50} \approx 60$ μm). However, both sediments had very low permeability, on the order of 10^{-15} m^2 (Table 2), which indicates that the fine fractions dominate the permeability of both sediments. Bulk metals concentrations were higher in C series sediments than in F series sediments (Table 2).

Table 2. Bulk Characteristics of PNS Sediments

experimental runs	F1–F3	C1–C3
porosity (%)	46.9 ± 0.3	37.0 ± 1.2
porewater salinity (‰)	29.5	29.3
permeability (m^2)	1.3 ± 1.2 × 10^{-15}	1.3 ± 0.3 × 10^{-15}
organic C (%)	1.94	1.77
AVS (μmol/g dry weight)	9.5 ± 1.9	22.2 ± 1.4
Cu (mg/kg dry weight)	256 ± 34	646 ± 76
Zn (mg/kg dry weight)	270 ± 67	618 ± 7
Fe (g/kg dry weight)	23.8 ± 0.9	30.3 ± 5.8
[Cu]/[Fe] (× 10^{-3} mol/mol)	9.48	18.8

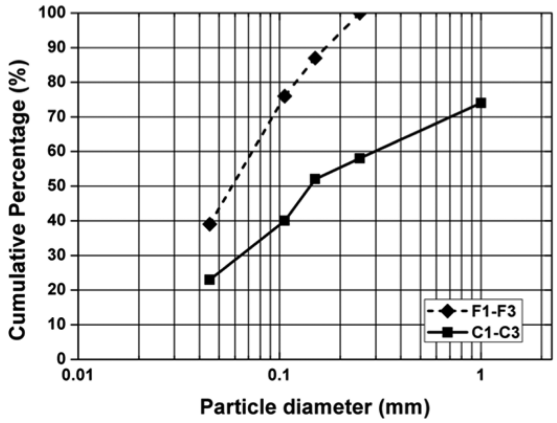

Figure 1. Sediment particle size distributions.

Metal Efflux to the Overlying Water. Overlying flow conditions influenced the efflux of metals to the overlying water in complicated ways. In experiments with the finer-grained sediments (F series), $[Cu]_d$ showed similar temporal patterns under all hydrodynamic conditions tested (Figure 2a). $[Cu]_d$ started at less than 15 nM and gradually approached ~50 nM in experiments F1, F2, and F3. Conversely, in experiments with coarser-grained sediments (C series), $[Cu]_d$ differed signifi-

DOI: 10.1021/acs.est.5b04576
Environ. Sci. Technol. XXXX, XXX, XXX–XXX

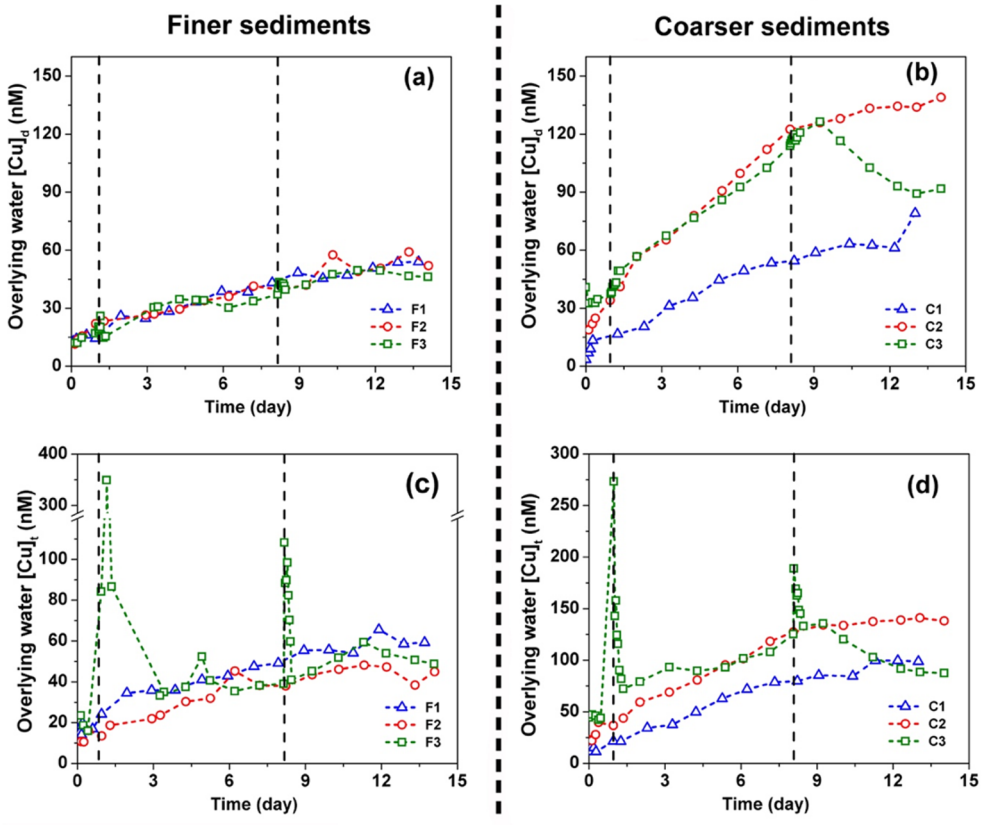

Figure 2. Release of Cu to the overlying water under varied hydrodynamic conditions. (a) Dissolved Cu concentrations ($[Cu]_d$) in experiments with finer-grained sediments. (b) Dissolved Cu concentrations ($[Cu]_d$) in experiments with coarser-grained sediments. (c) Total Cu concentrations ($[Cu]_t$) in experiments with finer-grained sediments. (d) Total Cu concentrations ($[Cu]_t$) in experiments with coarser-grained sediments. Episodic sediment resuspension events in experiments F3 (a, b) and C3 (c, d) are indicated by vertical dashed lines. Each sediment resuspension lasted 4 h (0.17 day).

cantly with overlying flow conditions (Figure 2b). In experiment C1 (3% of CS), $[Cu]_d$ gradually increased from 3 to 78 nM over the 14 day period of the experiments. In experiment C2 (50% of CS), $[Cu]_d$ rapidly increased from 18 to 123 nM within the first 8 days and then increased further to 140 nM over the remaining 6 days of the experiment. In experiment C3 (baseline 70% of CS, plus resuspensions), $[Cu]_d$ increased rapidly from 40 to 120 nM before the resuspension event on day 8 and then declined to 88 nM at day 14.

The proposed model, with the assumption of a constant $[Cu]_d$ in surficial porewater, reproduced the trends of overlying water $[Cu]_d$ measured in experiments with both finer- and coarser-grained sediments (Figure S9, SI). $[Cu]_d$ in the overlying water exponentially approached an upper limit S_0, suggesting the steady state was achieved. Overlying hydrodynamics exerted different impacts on S_0 between experiments with finer and coarser sediments. Experiments with finer sediments had similar values of S_0, but experiments with coarser sediments exhibited increasing S_0 with shear stresses, indicating that increasing hydrodynamic shear enhanced the liberation of Cu to the surficial porewater in the case of coarser sediments (Table S1, Supporting Information).

Total Cu concentrations ($[Cu]_t$) in the overlying water showed identical trends with $[Cu]_d$ during all periods of steady flow, but differed greatly during periods of resuspension (Figure 2c, d). Resuspension scoured surficial sediments to a depth of 1−2 mm (visual observation) and mobilized particle-associated Cu to the water column (Figure S4, Supporting Information). Particulate Cu concentrations in the water column ($[Cu]_p = [Cu]_t - [Cu]_d$) thus increased significantly during periods of resuspension. $[Cu]_p$ increased from 1.2 nM to 323 nM during the first resuspension period (day 1) and from 1.8 nM to 68 nM during the second resuspension period (day 8) in experiment F3, while $[Cu]_p$ increased from 9.4 nM to 235 nM during the first resuspension and from 11 nM to 73 nM during the second resuspension in experiment C3. However, these elevated Cu concentrations were highly transitory. $[Cu]_t$ and $[Cu]_p$ decreased rapidly following the cessation of sediment transport, and returned to preresuspension concentrations within 24 h.

4-day running average fluxes of dissolved Cu across the SWI were calculated from the rate of change of $[Cu]_d$ in the overlying water, obtained by linear least-squares fitting of 4 days of $[Cu]_d$ data normalized with the recirculating water volume and SWI area. Temporal variations of 4-day running average fluxes of dissolved Cu in all six experiments are shown in Figure 3. Effluxes of Cu remained similar over the course of all experiments with finer grained sediments (F1−F3), with an overall average efflux of ~1.9 μmol/m^2/d for the three experiments (Figure 3a). In contrast, 4-day running average fluxes in experiments with coarser grained sediments (C1−C3) showed significantly different trends (Figure 3b). Effluxes varied with overlying shear, with experiments C2 and C3 showing higher fluxes than C1 early in the experiments. Further, the effluxes in experiments C1−C3 decreased over time, indicating dissolved Cu in overlying water approached

DOI: 10.1021/acs.est.5b04576
Environ. Sci. Technol. XXXX, XXX, XXX−XXX

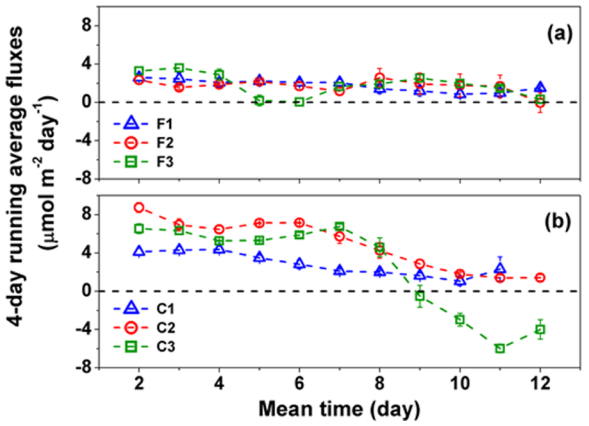

Figure 3. Four-day running average fluxes of $[Cu]_d$ in experiments with (a) finer-grained sediments and (b) coarser-grained sediments.

equilibrium late in the experiments. The efflux in experiment C3 became negative after the resuspension event, indicating net Cu sequestration in the sediments during this period corresponding to the observed decrease of Cu concentrations in the overlying water (Figure 2b,d).

Fe concentrations were also analyzed in overlying water samples from C-series experiments. All Fe in the overlying water was particulate, as dissolved Fe concentrations were below detection limit. Particulate Fe concentrations ($[Fe]_p$) in the overlying water for experiment C1−C3 are shown in Figure S5 (Supporting Information). In experiment C1 and C2, $[Fe]_p$ remained at low concentrations, corresponding to low levels of turbidity in the overlying water (Supporting Information Figure S4b). In experiment C3, sediment resuspension greatly increased $[Fe]_p$ in the overlying water. As with Cu, $[Fe]_p$ rapidly decreased to preresuspension levels following reduction of the shear to baseline shear stress. Further, $[Fe]_p$ was strongly correlated with $[Cu]_p$ but the $[Cu]_p$ /$[Fe]_p$ ratios varied over time (Figure S6, Supporting Information). Water column $[Cu]_p/[Fe]_p$ was slightly higher during the first resuspension ($6.3 \pm 0.2 \times 10^{-3}$) than during the second resuspension ($4.3 \pm 0.2 \times 10^{-3}$).

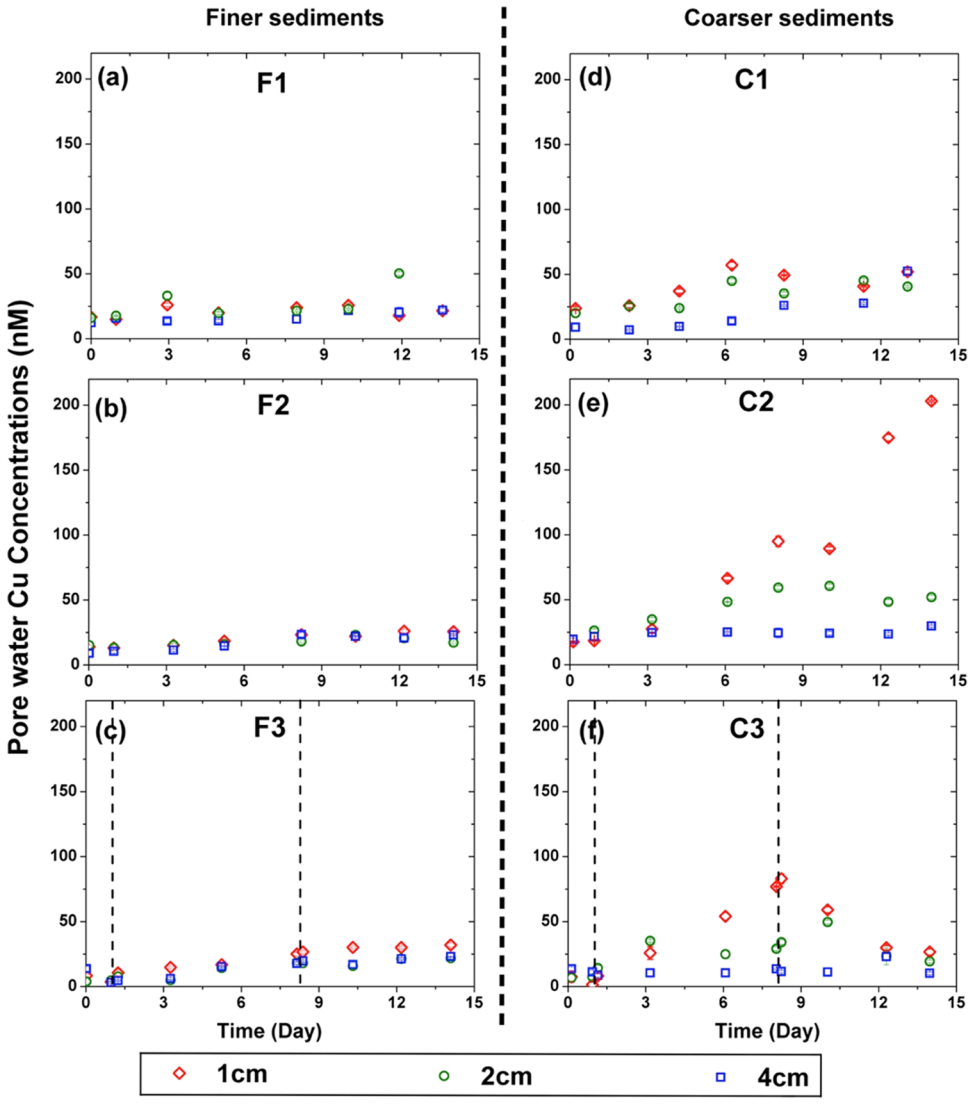

Figure 4. Temporal variations in porewater Cu concentrations in experiments with finer-grained sediments (a, b, c) and coarser grained sediments (d, e, f). Episodic sediment resuspension events in experiments F3 (c) and C3 (f) are indicated by vertical dashed lines. Each sediment resuspension lasted 4 h (0.17 day).

DOI: 10.1021/acs.est.5b04576
Environ. Sci. Technol. XXXX, XXX, XXX−XXX

Temporal Variations of Cu in Porewater. Porewater Cu concentrations in both sets of experiments showed similar response to hydrodynamic forcing. In experiments F1−F3 with finer-grained sediments (Figure 4a,b,c), Cu concentrations in porewater were uniform at all depths and were not significantly different between each treatment, suggesting that Cu mobilization and transport within the sediments were unaffected by overlying flow.

In experiments C1−C3 with coarser grained sediments (Figure 4d,e,f), porewater Cu concentrations showed higher temporal and spatial variability. Cu concentrations in porewater at 2 and 4 cm depth remained uniform throughout all experiments. However, Cu concentrations in near-surface porewater (1 cm depth) varied significantly with overlying flow conditions. In experiment C1 with 3% of CS, Cu concentrations in 1 cm porewater were constant with time. In experiment C2 with 50% of CS, Cu concentrations in 1 cm porewater increased rapidly from 20 to 200 nM. In experiment C3 with 70% CS and plus resuspension, Cu concentrations increased from 10 to 80 nM for the first 8 days and then decreased to 25 nM after the second resuspension event.

Dissolved Oxygen Profiles. Oxygen concentrations were relatively constant in the overlying water column but decreased near the SWI (Figure S10, Supporting Information). Oxygen rapidly decreased below the SWI and only penetrated less than 5 mm into the sediments in all experiments. In experiments with finer grained sediments (F1−F3), the DO profiles were similar under different hydrodynamic conditions, with an average penetration depth of 0.18 cm. Results from PROFILE showed that the oxygen consumption rates increased with depth in all three experiments. The diffusive O_2 fluxes at the SWI were similar for three experiments, with an average flux of 0.30 ± 0.06 μmol/cm^2/day (Table S2, Supporting Information). In experiments with coarser sediments (C1−C3), DO profiles varied under different hydrodynamic conditions. O_2 penetration depths were similar in experiment C1 (3% of CS) and C2 (50% of CS), but increased by a factor of 2 in experiment C3 (70% of CS plus resuspension), indicating that increasing hydrodynamic shear or/and sediment resuspension enhanced oxygen delivery into deeper sediments. Modeling results showed that O_2 was primarily consumed at the base of the O_2 penetration region.

Fe^{2+} Fluxes in Porewater. Dissolved Fe concentrations in porewater in experiments C1−C3 also showed varied patterns. In experiments C1−C3, porewater Fe concentrations were uniform over depth at the initiation of experiments because the sediments had been homogenized prior to emplacement in the Gust chambers (Figure S11, Supporting Information). Dissolved Fe in the top 2 cm rapidly decreased (within 2 days) after the initiation of experiments, whereas dissolved Fe at 4 cm depth remained approximately constant throughout the course of experiments. The strong Fe^{2+} concentration gradients in the porewater indicated Fe^{2+} fluxes toward the SWI. Diffusion of Fe^{2+} occurred slowly in porewater, with an effective diffusion coefficient of 8.9×10^{-7} cm^2/s.[43,44] Assuming Fe^{2+} was oxidized and precipitated as iron oxy-hydroxide at the base of the oxic region (0.2−0.4 cm below the SWI), the approximate time for Fe^{2+} diffusion in experiments C1−C3 was 2.3−4.2, 17−21, and 84−94 days from depths 1, 2, and 4 cm into the oxic region, respectively (Table S3, Supporting Information). The average Fe^{2+} fluxes into oxic regions were $7.5 \pm 3.1 \times 10^{-3}$, $6.6 \pm 3.4 \times 10^{-3}$, and $11 \pm 6 \times 10^{-3}$ μmol cm^{-2} day^{-1} respectively (Table S4, Supporting Information). All Fe fluxes were significantly smaller than the diffusive oxygen fluxes (Table S2, Supporting Information), indicating nearly complete oxidation of Fe^{2+} in the oxic region. Further, the existence of Fe^{2+} gradients in the porewater throughout the experiments indicated continuous supply of iron from the deeper sediments into the oxic region.

DISCUSSION

Overlying flow influences surface-porewater exchange, biogeochemical zonation, and the fate of contaminants in sediments.[17,45,46] Most studies of surface-porewater exchange have focused on fluvial systems, where the sediments are typically highly permeable. However, porewater transport in fine sediments with low permeability is generally considered to be dominated by diffusion, and thus the effects of overlying hydrodynamics are often neglected in assessments of metals transport.[17] Here, we observed that increasing hydrodynamic shear on the SWI enhanced the penetration of oxygen into sediments, increased Cu concentrations in surficial porewater, and facilitated the release of dissolved Cu to the overlying water in experiments with low-permeability, but relatively heterogeneous sediments (C1−C3). These observations suggest that hydrodynamic shear is likely to play a critical role in controlling the mobilization and overall efflux of metals even in sediments with permeability as low as 10^{-15} m^2.

We observed lower and more constant fluxes of dissolved Cu in the overlying water between different hydrodynamic treatments in sediments that had similarly low permeability, but were more homogeneous (F1−F3) (Table S5, Supporting Information). The observed Cu fluxes (−0.03−3.95 μmol/m^2/day) were similar to the range of benthic diffusive fluxes observed in other studies (−0.07−3.60 μmol/m^2/day) (Table S5, Supporting Information), suggesting that Cu fluxes were predominantly diffusive under all hydrodynamic conditions tested. These findings indicate that sediment heterogeneity (e.g., size distribution) influences the efflux of dissolved Cu from low-permeability sediments.

Sediment resuspension also exerted diverse effects on metal mobilization. During resuspension, overlying water turbidity and total Cu concentrations increased dramatically as a result of mobilization of metals-rich sediment particles to the overlying water column (Figure 2 and Figure S4, Supporting Information). Similarly high particulate Cu effluxes were observed during resuspension of both sediments (Table S6, Supporting Information). However, the residual effects on overlying water and porewater chemistry differed between sediment types. In experiments with coarser sediments (C3), Cu concentrations in both overlying water and porewater decreased gradually after the end of the second resuspension (Figure 3b, d and Figure 4f). Complementary analysis of dissolved and particulate metals suggested that the liberated Cu was scavenged by oxidized Fe particles. Reductive dissolution of Fe species in deeper sediments continuously supplied dissolved Fe^{2+} toward the surficial sediments (Supporting Information Figure S11), where it was readily oxidized by oxygen from the overlying water. Diffusion of $Fe^{(II)}$ occurred very slowly in the porewater (Supporting Information Table S3), leading to a few days lag of production and transport of $Fe^{(III)}$ oxy-hydroxide precipitates into the surficial region. Freshly formed Fe rich particles are known to provide reactive surfaces for Cu adsorption and immobilization.[31] Therefore, it appears that the Fe rich particles liberated during the second resuspension event were responsible for the scavenging of dissolved Cu in

DOI: 10.1021/acs.est.5b04576
Environ. Sci. Technol. XXXX, XXX, XXX−XXX

the overlying water and porewater. This hypothesis was further supported by the high correlations between particulate Fe and particulate Cu during the two resuspension events (Figure S6, Supporting Information). A higher [Cu]/[Fe] ratio ($6.3 \pm 0.2 \times 10^{-3}$) was observed for the first resuspension while a lower [Cu]/[Fe] ratio ($4.3 \pm 0.2 \times 10^{-3}$) was observed for the second resuspension. The attenuation of the [Cu]/[Fe] ratio could potentially be explained by mixing of Fe-rich particles with much lower [Cu]/[Fe] ratio ($[Cu]_{PW}/[Fe]_{PW}$ ratio at a depth of 1 cm = $5.9 \pm 6.5 \times 10^{-4}$) liberated during the second resuspension event.

Studying the coupled effects of biogeochemical and hyporheic processes on metal mobilization near the SWI are challenging because of the strong hydrodynamic and biogeochemical gradients.[47,48] Biogeochemical reactions controlling the partitioning of metals between sediment particles and porewater occur at sediment grain surfaces while hyporheic processes transport solutes over a wide range of spatial scale.[49] Sampling methods commonly applied to capture the effects of flow dynamics usually do not sufficiently resolve concentration gradients for quantifying biogeochemical reaction rates. In the current study, we used a simple mass balance model to represent the release of dissolved Cu to the water column. Assumption of constant $[Cu]_{d,SPW}$ was sufficient to reproduce the observed temporal patterns of $[Cu]_d$ in the overlying water, indicating that the reservoir of Cu in surficial sediment was not significantly depleted during the 14-day period of observation. In low-permeability sediments, Cu concentrations in surficial porewater are controlled by the competition between liberation of Cu from the solid phase to the porewater and transport of dissolved Cu from the porewater to the overlying water column. Resupply of $[Cu]_d$ from sediment to porewater is a much faster process (a few hours)[50] than the time scale of transport across the SWI (a few days), and thus the steady state of $[Cu]_{d,SPW}$ achieves shortly after the experiment initiated. Hence the assumption of constant $[Cu]_{d,SPW}$ holds in eq 3 and this model can be used to quantify contaminants efflux in other highly contaminated, low-permeability sediments where ongoing fluxes do not significantly deplete the source of contamination over time scales of interest.

The mass balance model represents efflux of Cu to the water column in terms of two parameters—the interfacial exchange rate (α_{eff}) and surficial porewater Cu conentrations (S_0). Increasing α_{eff} corresponds to increasing release rates of Cu to the overlying water and decreasing time for $[Cu]_{d,OW}$ to approach to equilibrium. Increasing S_0 not only yields greater equilibrium Cu concentration in the water column, but also a greater rate of Cu efflux from the sediments early in the experiments. S_0 depends on the dynamic balance between resupply of Cu from the sediment phase and transport of Cu in the porous sediments. While resupply of dissolved Cu from the sediments is controlled by dissolution of metal-containing mineral phases, the transport of Cu is regulated by properties of both the porewater flow and the solid matrix. The effective exchange rate of solutes between porewater and overlying water, α_{eff}, is also regulated by both sediment properties and overlying hydrodynamics. In permeable sediments, increasing hydrodynamic shear on the sediment surface favors advective porewater flow and enhances the exchange rate.[22,45] In low-permeability sediments, molecular diffusion dominates porewater motion and associated solute transport within the sediments.[15] Overlying hydrodynamics also influences solute exchange in such sediments by changing the diffusive boundary layer (DBL) above the sediments.[51] Increasing hydrodynamic shear decreases the thickness of DBL, sharpens solute concentration gradients within the DBL, and increases solute exchange rates across the DBL.[52] In addition, turbulence in the bulk flow imposes vortices that sweep and eject water into and out of the DBL, which also increases flux across the DBL.[53,54]

Overall, the current study demonstrated the coupled effects of overlying hydrodynamics and sediment geochemistry on mobility of metals (Figure S13, Supporting Information). Previous studies showed that diffusion of oxygen from the overlying water column oxidizes surficial sediments, changes metal solubility, and releases metals to porewater and overlying water.[32,55] Here, we observed that oxygen penetrated into sediments, resulting in significantly decreased AVS (Figure S12, Supporting Information) and increased Cu mobility in these surficial sediments, and liberation of Cu to the porewater and overlying water. Increased hydrodynamic forcing enhanced mass transfer across the SWI and promoted liberation of Cu from the surficial porewater. The mobility of Cu was also strongly coupled with Fe chemistry. Particulate Cu was highly correlated with particulate Fe and was mobilized/immobilized when sediment resuspension events initiated/ceased.

Implications for Assessment of Contaminated Sites. In low-permeability sediments, such as the estuarine sediments used here, solute transport in porewater is generally considered to occur predominately by diffusion.[17,22,25] However, our results clearly show that hydrodynamic shear can enhance the transport of oxygen, the mobilization of Cu to porewater, and the overall efflux of dissolved Cu to the overlying water column even in low-permeability sediments.[56] We also found that flows that are sufficiently high to induce sediment resuspension dramatically increase particulate metals concentrations on a transient basis, and can also accelerate the liberation of dissolved metals from porewater. Many estuarine sediments are subject to highly variable hydrodynamic conditions, including regular tidal fluctuations and episodic floods and storms.[57] Temporal variability in overlying hydrodynamic processes, including the potential for sediment resuspension, should therefore be expected to strongly influence the long-term mobility and efflux of metals in estuarine sediments.

While the current study used homogenized sediment beds, natural estuarine sediments tend to have more structural heterogeneities. Water flows preferentially remove and transport finer sediments, leading to formation of coarser surficial or buried sediment layers.[58] In addition, transport and deposition of suspended sediments result in development of bed forms that vary geometrically in size and shape.[59] These structural heterogeneities are known to produce spatially variable hyporheic exchange patterns and induce higher interfacial exchange fluxes.[45,58,60] The effects that hydrodynamic forcing mobilizes metals are thus likely to be even more prominent in such sediments.

Investigation of contaminated sediment sites typically involves a sequence of approaches: development of a conceptual site model (CSM), screening assessment, characterization of exposure and effects, and identification of remedial actions.[61] Identifying the critical process that influence the mobility of metals is an essential step in developing a CSM. This is complicated in dynamic sites exhibiting spatially and temporally variable patterns of metal fluxes, as site assessments typically use a low density and frequency of sampling.[31] Effects of time-variable flow forcing on the release and effects of contaminants from sediments are thus likely to be omitted from

DOI: 10.1021/acs.est.5b04576
Environ. Sci. Technol. XXXX, XXX, XXX−XXX

CSMs. This study emphasizes the need to establish shear-efflux relationships for site sediments and provides a framework for determining the shear-efflux relations by measuring metal efflux under different shear stresses. With the ability to impose a wide range of precisely controlled hydrodynamic shears on sediments, the Gust mesocosm system could be used *in situ* or *ex situ* to determine the empirical correlations between shear stresses and metal effluxes. Flow-induced metal effluxes then need to be estimated based on historic hydrodynamic conditions at site and risks of omitting such hydrodynamic processes can be identified and corresponding risk factors can be incorporated in site assessments.

In addition, current approaches for assessing bioavailability and toxicity of metals in sediments employ bulk sediment characterizations, often relying on batch organism exposure in a laboratory setting in combination with equilibrium partitioning models that attribute toxicity to the presence of dissolved metals in porewater.[62] These approaches will miss ecological uptake and risk factors that result from interactions between flow, metals chemistry, and biological processes. Based on the results presented here, assessments of contaminated sediment bioavailability and toxicity should also include measurements of the effects of flow forcing in concert with bioturbation and bioirrigation in characterizations of exposure and effects.

■ ASSOCIATED CONTENT

Supporting Information

The Supporting Information is available free of charge on the ACS Publications website at DOI: 10.1021/acs.est.5b04576.

Additional explanations, tables, and figures as noted in the text can be found in Supporting Information (PDF)

■ AUTHOR INFORMATION

Corresponding Authors

*(J.-F.G.) Phone: 847-467-1376; fax: 847-491-4011; e-mail: jf-gaillard@northwestern.edu.

*(A.P.) Phone: 847-491-9902; fax: 847-491-4011; e-mail: a-packman@northwestern.edu.

Notes

The authors declare no competing financial interest.

■ ACKNOWLEDGMENTS

This research was supported by the SERPD program (ER-1745). M.X. and N.W. were supported by grant from Chinese Scholarship Council (CSC). We also thank the editor Xiangdong Li and four anonymous reviewers for their constructive comments to improve the manuscript.

■ REFERENCES

(1) McLusky, D. *The Estuarine Ecosystem*; Springer Science & Business Media, 2013.

(2) Ji, Z.-G. *Hydrodynamics and Water Quality: Modeling Rivers, Lakes, And Estuaries*; John Wiley & Sons, .

(3) Nixon, S.; Oviatt, C.; Frithsen, J.; Sullivan, B. Nutrients and the productivity of estuarine and coastal marine ecosystems. *J. Limnol. Soc. South. Afr.* **1986**, *12* (1−2), 43−71.

(4) Ridgway, J.; Shimmield, G. Estuaries as repositories of historical contamination and their impact on shelf seas. *Estuarine, Coastal Shelf Sci.* **2002**, *55* (6), 903−928.

(5) Flemming, C.; Trevors, J. Copper toxicity and chemistry in the environment: a review. *Water, Air, Soil Pollut.* **1989**, *44* (1−2), 143−158.

(6) Lossin, A.; Westhoff, F.-J. The production and application of cuprous oxide and cupric hydroxide. *JOM* **1997**, *49* (10), 38−39.

(7) Eggleton, J.; Thomas, K. V. A review of factors affecting the release and bioavailability of contaminants during sediment disturbance events. *Environ. Int.* **2004**, *30* (7), 973−980.

(8) Hong, Y. S.; Kinney, K. A.; Reible, D. D. Effects of cyclic changes in pH and salinity on metals release from sediments. *Environ. Toxicol. Chem.* **2011**, *30* (8), 1775−1784.

(9) Van Cappellen, P.; Gaillard, J.-F. Biogeochemical dynamics in aquatic sediments. *Rev. Mineral. Geochem.* **1996**, *34* (1), 335−376.

(10) Borch, T.; Kretzschmar, R.; Kappler, A.; Cappellen, P. V.; Ginder-Vogel, M.; Voegelin, A.; Campbell, K. Biogeochemical redox processes and their impact on contaminant dynamics. *Environ. Sci. Technol.* **2009**, *44* (1), 15−23.

(11) Aller, R. C., The effects of macrobenthos on chemical properties of marine sediment and overlying water. In *Animal-Sediment Relations*; Springer, 1982.

(12) Pischedda, L.; Poggiale, J.-C.; Cuny, P.; Gilbert, F. Imaging oxygen distribution in marine sediments. The importance of bioturbation and sediment heterogeneity. *Acta Biotheor.* **2008**, *56* (1−2), 123−135.

(13) Glud, R.; Ramsing, N. B.; Gunderson, J. K.; Klimant, I. Planar optodes, a new tool for fine scale measurements of two-dimensional O2 distribution in benthic communities. *Mar. Ecol.: Prog. Ser.* **1996**, *140*, 217−226.

(14) Zhu, Q.; Aller, R. C.; Fan, Y. High-performance planar pH fluorosensor for two-dimensional pH measurements in marine sediment and water. *Environ. Sci. Technol.* **2005**, *39* (22), 8906−8911.

(15) Huettel, M.; Webster, I. T., Porewater flow in permeable sediments. In *The Benthic Boundary Layer: Transport Processes and Biogeochemistry*; Oxford University Press: New York, 2001; pp 144−179.

(16) Kimball, B. A.; Broshears, R. E.; Bencala, K. E.; McKnight, D. M. Coupling of hydrologic transport and chemical reactions in a stream affected by acid mine drainage. *Environ. Sci. Technol.* **1994**, *28*, 2065−2073.

(17) Huettel, M.; Ziebis, W.; Forster, S.; Luther Iii, G. W. Advective transport affecting metal and nutrient distributions and interfacial fluxes in permeable sediments. *Geochim. Cosmochim. Acta* **1998**, *62* (4), 613−631.

(18) Nagorski, S.; Moore, J. Arsenic mobilization in the hyporheic zone of a contaminated stream. *Water Resour. Res.* **1999**, *35* (11), 3441−3450.

(19) Boudreau, B. P.; Jørgensen, B. B. *The Benthic Boundary Layer: Transport Processes and Biogeochemistry*; Oxford University Press: Oxford ; New York, 2001; p xii, 404.

(20) Ren, J.; Packman, A. I. Modeling of simultaneous exchange of colloids and sorbing contaminants between streams and streambeds. *Environ. Sci. Technol.* **2004**, *38* (10), 2901−2911.

(21) Ren, J. H.; Packman, A. I. Coupled stream-subsurface exchange of colloidal hematite and dissolved zinc, copper, and phosphate. *Environ. Sci. Technol.* **2005**, *39* (17), 6387−6394.

(22) Boano, F.; Harvey, J.; Marion, A.; Packman, A.; Revelli, R.; Ridolfi, L.; Wörman, A. Hyporheic flow and transport processes: Mechanisms, models, and biogeochemical implications. *Rev. Geophys.* **2014**, *52* (4), 603−679.

(23) Elliott, A. H.; Brooks, N. H. Transfer of nonsorbing solutes to a streambed with bed forms: Theory. *Water Resour. Res.* **1997**, *33* (1), 123−136.

(24) Elliott, A. H.; Brooks, N. H. Transfer of nonsorbing solutes to a streambed with bed forms: Laboratory experiments. *Water Resour. Res.* **1997**, *33* (1), 137−151.

(25) Huettel, M.; Webster, I. T., Porewater flow in permeable sediments. In *The Benthic Boundary Layer: Transport Processes and Biogeochemistry*; Oxford University Press: New York, 2001.

(26) Thibodeaux, L. J.; Boyle, J. D. Bedform-generated convective transport in bottom sediment. *Nature* **1987**, *325*, 341−343.

(27) Ospina-Álvarez, N.; Caetano, M.; Vale, C.; Santos-Echeandía, J.; Bernárdez, P.; Prego, R. Exchange of nutrients across the sediment−

DOI: 10.1021/acs.est.5b04576
Environ. Sci. Technol. XXXX, XXX, XXX−XXX

water interface in intertidal ria systems (SW Europe). *J. Sea Res.* **2014**, *85*, 349−358.
(28) Vanderborght, J. P.; Wollas, R.; Bitten, G. Kinetic models of diagenesis in disturbed sediments. Part 1. Mass transfer properties and silica diagenesis. *Limnol. Oceanogr.* **1977**, *22* (5), 787−793.
(29) Lohse, L.; Epping, E.; Helder, W.; Van Raaphorst, W. Oxygen pore water profiles in continental shelf sediments of the North Sea: turbulent versus molecular diffusion. *Mar. Ecol.: Prog. Ser.* **1996**, *145*, 63−75.
(30) Kerner, M.; Wallmann, K. Remobilization events involving Cd and Zn from intertidal flat sediments in the Elbe estuary during the tidal cycle. *Estuarine, Coastal Shelf Sci.* **1992**, *35* (4), 371−393.
(31) Burton, G. A. Metal bioavailability and toxicity in sediments. *Crit. Rev. Environ. Sci. Technol.* **2010**, *40* (9−10), 852−907.
(32) Xie, M.; Jarrett, B. A.; Da Silva-Cadoux, C.; Fetters, K. J.; Burton, G. A.; Gaillard, J.-F.; Packman, A. I. Coupled effects of hydrodynamics and biogeochemistry on Zn mobility and speciation in highly contaminated sediments. *Environ. Sci. Technol.* **2015**, *49* (9), 5346−5353.
(33) Allen, H. E. e. a., Determination of acid volatile sulfides and simultaneously extractable metals in sediment. In U.S. EPA, 1991.
(34) Element, C. A. S., Method 3051A. Microwave assisted acid digestion of sediments, sludges, soils, and oils. 2007.
(35) Thomsen, L.; Gust, G. Sediment erosion thresholds and characteristics of resuspended aggregates on the western European continental margin. *Deep Sea Res., Part I* **2000**, *47* (10), 1881−1897.
(36) Seeberg-Elverfeldt, J.; Schlüter, M.; Feseker, T.; Kölling, M. Rhizon sampling of pore waters near the sediment/water interface of aquatic systems. *Limnol. Oceanogr.: Methods* **2005**, *3*, 361−371.
(37) Dickens, G. R.; Koelling, M.; Smith, D. C.; Schnieders, L. Rhizon Sampling of Pore Waters on Scientific Drilling Expeditions: An Example from the IODP Expedition 302, Arctic Coring Expedition (ACEX). *Sci. Drill.* **2007**, *4*, 22−25.
(38) Shotbolt, L. Pore water sampling from lake and estuary sediments using Rhizon samplers. *Journal of Paleolimnology* **2010**, *44* (2), 695−700.
(39) Stookey, L. L. Ferrozine—a new spectrophotometric reagent for iron. *Anal. Chem.* **1970**, *42* (7), 779−781.
(40) Viollier, E.; Inglett, P. W.; Hunter, K.; Roychoudhury, A. N.; Van Cappellen, P. The ferrozine method revisited: Fe (II)/Fe (III) determination in natural waters. *Appl. Geochem.* **2000**, *15* (6), 785−790.
(41) Berg, P.; Risgaard-Petersen, N.; Rysgaard, S. Interpretation of measured concentration profiles in sediment pore water. *Limnol. Oceanogr.* **1998**, *43* (7), 1500−1510.
(42) Webb, S. M.; Leppard, G. G.; Gaillard, J.-F. Zinc speciation in a contaminated aquatic environment: characterization of environmental particles by analytical electron microscopy. *Environ. Sci. Technol.* **2000**, *34* (10), 1926−1933.
(43) Yuan-Hui, L.; Gregory, S. Diffusion of ions in sea water and in deep-sea sediments. *Geochim. Cosmochim. Acta* **1974**, *38* (5), 703−714.
(44) Boudreau, B. P. The diffusive tortuosity of fine-grained unlithified sediments. *Geochim. Cosmochim. Acta* **1996**, *60* (16), 3139−3142.
(45) Packman, A. I.; Salehin, M.; Zaramella, M. Hyporheic exchange with gravel beds: basic hydrodynamic interactions and bedform-induced advective flows. *Journal of Hydraulic Engineering* **2004**, *130* (7), 647−656.
(46) Bencala, K. E. Simulation of solute transport in a mountain pool-and-riffle stream with a kinetic mass transfer model for sorption. *Water Resour. Res.* **1983**, *19* (3), 732−738.
(47) Meysman, F.; Galaktionov, O.; Cook, P.; Janssen, F.; Huettel, M.; Middelburg, J. Quantifying biologically and physically induced flow and tracer dynamics in permeable sediments. *Biogeosciences Discussions* **2006**, *3* (6), 1809−1858.
(48) Zarnetske, J. P.; Haggerty, R.; Wondzell, S. M.; Bokil, V. A.; González-Pinzón, R., Coupled transport and reaction kinetics control the nitrate source-sink function of hyporheic zones. *Water Resour. Res.* **2012**, *48*, (11).n/a10.1029/2012WR011894
(49) O'Connor, B. L.; Harvey, J. W., Scaling hyporheic exchange and its influence on biogeochemical reactions in aquatic ecosystems. *Water Resour. Res.* **2008**, *44*, (12).n/a10.1029/2008WR007160
(50) Harper, M. P.; Davison, W.; Zhang, H.; Tych, W. Kinetics of metal exchange between solids and solutions in sediments and soils interpreted from DGT measured fluxes. *Geochim. Cosmochim. Acta* **1998**, *62* (16), 2757−2770.
(51) Huettel, M.; Røy, H.; Precht, E.; Ehrenhauss, S., Hydrodynamical impact on biogeochemical processes in aquatic sediments. In *The Interactions between Sediments and Water*; Springer, 2003; pp 231−236.
(52) Clark, M. M. *Transport Modeling for Environmental Engineers and Scientists*: John Wiley & Sons, 2012.
(53) O'Connor, B. L.; Hondzo, M. Dissolved oxygen transfer to sediments by sweep and eject motions in aquatic environments. *Limnol. Oceanogr.* **2008**, *53* (2), 566−578.
(54) Boudreau, B. P. Solute transport above the sediment-water interface. *Benthic boundary layer: Transport processes and biogeochemistry* **2001**, 104−126.
(55) Simpson, S. L.; Ward, D.; Strom, D.; Jolley, D. F. Oxidation of acid-volatile sulfide in surface sediments increases the release and toxicity of copper to the benthic amphipod Melita plumulosa. *Chemosphere* **2012**, *88* (8), 953−961.
(56) Gundersen, J. K.; Jorgensen, B. B. Microstructure of diffusive boundary layers and the oxygen uptake of the sea floor. *Nature* **1990**, *345* (6276), 604−607.
(57) Kalnejais, L. H.; Martin, W. R.; Signell, R. P.; Bothner, M. H. Role of sediment resuspension in the remobilization of particulate-phase metals from coastal sediments. *Environ. Sci. Technol.* **2007**, *41* (7), 2282−2288.
(58) Packman, A. I.; Marion, A.; Zaramella, M.; Chen, C.; Gaillard, J.-F.; Keane, D. T. Development of layered sediment structure and its effects on pore water transport and hyporheic exchange. *Water, Air, Soil Pollut.: Focus* **2006**, *6* (5−6), 433−442.
(59) Balachandar, R.; Reddy, H. P. *Bed Forms and Flow Mechanisms Associated with Dunes*. INTECH Open Access Publisher: 2011.
(60) Cardenas, M. B.; Wilson, J.; Zlotnik, V. A., Impact of heterogeneity, bed forms, and stream curvature on subchannel hyporheic exchange. *Water Resour. Res.* **2004**, *40*, (8), 10.1029/2004WR003008
(61) Sorell, T.; McEvoy, K. Incorporating Bioavailability Considerations Into the Evaluation of Contaminated Sediment Sites. *Remediation Journal* **2013**, *23* (1), 63−72.
(62) Di Toro, D. M.; Zarba, C. S.; Hansen, D. J.; Berry, W. J.; Swartz, R. C.; Cowan, C. E.; Pavlou, S. P.; Allen, H. E.; Thomas, N. A.; Paquin, P. R. Technical basis for establishing sediment quality criteria for nonionic organic chemicals using equilibrium partitioning. *Environ. Toxicol. Chem.* **1991**, *10* (12), 1541−1583.

DOI: 10.1021/acs.est.5b04576
Environ. Sci. Technol. XXXX, XXX, XXX−XXX